

## A SUPPLEMENTARY MATERIAL

In the supplementary material, we provide the following additional details:

- A complete proof of the posterior energy formulation presented in the main paper.
- Visualizations of the line fields along with the corresponding images.
- Additional qualitative and quantitative results to further support our findings.
- Usage of LLM

### PROOF OF THE MRF ENERGY OF THE POSTERIOR:

**Theorem:** Let the prior distribution  $\mathbb{P}(X = \omega)$  be a Gibbs distribution defined over a neighborhood  $\{S, \mathcal{G}\}$  with corresponding energy  $\mathcal{E}$  and potential  $\{V_C\}$ :  $\mathbb{P}(X = \omega) = e^{-\mathcal{E}(\omega)}/Z$ ,  $\mathcal{E}(\omega) = \sum_C V_C(\omega)$ , where  $\omega = (f, l)$ . Then, for any fixed observation  $g$ , the posterior distribution  $\mathbb{P}(X = \omega | G = g)$  is also a Gibbs distribution, defined over the neighborhood system  $\{S, \mathcal{G}^P\}$ , with the posterior energy function given by:

$$\mathcal{E}^P(f, l) = \mathcal{E}(f, l) + \frac{1}{2\sigma^2} \|\mu - \Phi(g, \mathcal{D}_\psi(H(F)))\|^2 \quad (14)$$

where  $\mathcal{G}^P$  denotes the extended neighborhood system defined as:

$$\mathcal{G}_s^P = \begin{cases} \mathcal{G}_s, & \text{if } s \in D_m \\ \mathcal{G}_s \cup \mathcal{H}_s^2 \setminus \{s\}, & \text{if } s \in Z_m \end{cases} \quad (15)$$

*proof:* We start with the definition of the degradation operator,  $G = \phi(H(F)) \odot \mathcal{N}$ , where  $\mathcal{N} \sim \mathcal{N}(\mu, \sigma^2)$  is additive white Gaussian noise, assumed independent of the MRF  $\{S, \mathcal{G}\}$ . The operation  $\odot$  is assumed to be invertible, such that we can write  $\mathcal{N} = \Phi(G, \mathcal{D}_\psi(H(F))) = \{\Phi_s, s \in Z_m\}$ . Let  $\mathcal{H}_s, s \in Z_m$  denote the set of pixels that affect the blurred image  $H(F)$  at  $s$ . For instance  $\mathcal{H}_s$  can be a  $3 \times 3$  window centered at  $s$ .  $\{\Phi_s, s \in Z_m\}$  depends only on  $g_s$  and  $\{f_t : t \in \mathcal{H}_s\}$ . Because of the shift invariance of  $H$ , these neighborhoods satisfy  $\mathcal{H}_{r+s} = s + \mathcal{H}_r$  where  $\mathcal{H}_r \subseteq Z_m, s+r \in Z_m$  and  $s + \mathcal{H}_r$  intersects  $Z_m$ . If  $\{\mathcal{H}_s\}$  is symmetric such that  $r \in \mathcal{H}_0 \implies -r \in \mathcal{H}_0$ , then the collection  $\{\mathcal{H}_s \setminus \{s\}, s \in Z_m\}$  forms a valid neighborhood system over  $Z_m$ . Let  $\mathcal{H}^2$  define the second-order neighborhood system as:

$$\mathcal{H}_s^2 = \cup_{r \in \mathcal{H}_s} \mathcal{H}_r, s \in Z_m \quad (16)$$

Then  $\{\mathcal{H}_s^2 \setminus \{s\}, s \in Z_m\}$  also defines a neighborhood system. We define the posterior neighborhood system  $\{\mathcal{G}^P = \mathcal{G}_s^P, s \in S\}$  as,

$$\mathcal{G}_s^P = \begin{cases} \mathcal{G}_s, & \text{if } s \in D_m \\ \mathcal{G}_s \cup \mathcal{H}_s^2 \setminus \{s\}, & \text{if } s \in Z_m \end{cases} \quad (17)$$

Applying Bayes' rule, we express the posterior as:

$$\mathbb{P}(X = \omega | G = g) = \frac{\mathbb{P}(G = g | X = \omega) \cdot \mathbb{P}(X = \omega)}{\mathbb{P}(G = g)} \quad (18)$$

$\forall \omega = (f, l)$  and each  $g$ . Assuming  $\mathbb{P}(X = \omega) = e^{-\mathcal{E}(\omega)}/Z$ , the likelihood term becomes:

$$\begin{aligned} \mathbb{P}(G = g | X = \omega) &= \mathbb{P}(\mathcal{D}_\psi(H(X)) \odot \mathcal{N} = g | X = \omega) \\ &= \mathbb{P}(\mathcal{N} = \Phi(g, \mathcal{D}_\psi(H(X)))) \\ &= (2\pi\sigma^2)^{-M/2} \exp\left\{-\frac{1}{2\sigma^2} \|\mu - \Phi\|^2\right\} \end{aligned} \quad (19)$$

Again,  $\mathbb{P}(X = \omega | G = g) = e^{-\mathcal{E}^P(\omega)}/Z^P$ .

**Case  $s \in Z_m$ :** The term  $\Phi$  does not cancel out.  $\Phi(g, \mathcal{D}_\psi(H(F))) = \{\Phi_s, s \in Z_m\}$ .

Taking Eq 18 and Eq. 19 we can write,

$$\mathbb{P}(X = \omega | \mathcal{N} = \Phi) \propto \mathbb{P}(\mathcal{N} = \Phi | X = \omega) \cdot \mathbb{P}(X = \omega). \quad (20)$$

Taking the negative logarithm, the posterior energy becomes:

$$\mathcal{E}^P(f, l) = -\log \mathbb{P}(\mathcal{N} = \Phi \mid X = \omega) - \log \mathbb{P}(X = \omega). \quad (21)$$

From Eq. 19 we get,

$$-\log \mathbb{P}(\mathcal{N} = \Phi \mid X = \omega) = \frac{1}{2\sigma^2} \sum_{r \in Z_m} (\Phi_r(g_r; f_t, t \in \mathcal{H}_r) - \mu)^2 + \text{const.} \quad (22)$$

Combining both terms, the full posterior energy becomes:

$$\mathcal{E}^P(f, l) = \sum_C V_C(f, l) + \frac{1}{2\sigma^2} \sum_{r \in Z_m} (\Phi_r(g_r; f_t, t \in \mathcal{H}_r) - \mu)^2. \quad (23)$$

$$\begin{aligned} \mathbb{P}(F_s = f_s \mid F_r = f_r, r \neq s, r \in Z_m, L = l, G = g) &= \frac{e^{-\mathcal{E}^P(\omega)} / Z^P}{\sum_{f_s} e^{-\mathcal{E}^P(\omega)} / Z^P} = \frac{e^{-\mathcal{E}(\omega)} / Z}{\sum_{f_s} e^{-\mathcal{E}(\omega)} / Z} \\ &= \frac{e^{-\mathcal{E}(f, l) - \frac{1}{2\sigma^2} \sum_{r \in Z_m} (\Phi_r - \mu)^2}}{\sum_{f_s} e^{-\mathcal{E}(f, l) - \frac{1}{2\sigma^2} \sum_{r \in Z_m} (\Phi_r - \mu)^2}} \quad (24) \end{aligned}$$

$$\begin{aligned} \Rightarrow \mathcal{E}^P(f, l) &= \sum_{C: s \in C} V_C(f, l) + \frac{1}{2\sigma^2} \sum_{r: s \in \mathcal{H}_r} (\Phi_r(g_r; f_t, t \in \mathcal{H}_r) - \mu)^2 \\ &\quad + \sum_{C: s \notin C} V_C(f, l) + \frac{1}{2\sigma^2} \sum_{r: s \notin \mathcal{H}_r} (\Phi_r(g_r; f_t, t \in \mathcal{H}_r) - \mu)^2 \quad (25) \end{aligned}$$

It can be seen that the last two terms in 25 does not involve  $f_s$  and the ratio in 24 depends only on the first two terms of 25. The first two terms depends only on the coordinate  $(f, l)$  for the sites in  $\mathcal{G}_s \{s \in C \implies C \subseteq \mathcal{G}_s\}$  and the second term only on the sites in  $= \cup_{r: s \in \mathcal{H}_r} \mathcal{H}_s = \cup_{r \in \mathcal{H}_s} \mathcal{H}_r = \mathcal{H}_s^2$ . Hence we can say,  $\mathcal{G}_s^P = \mathcal{G}_s \cup \mathcal{H}_s^2 \setminus \{s\}$ .

Case  $s \in D_m$ :

$$\begin{aligned} \mathbb{P}(L_s = l_s \mid L_r = l_r, r \neq s, r \in D_m, F = f, G = g) \\ = \frac{e^{-\mathcal{E}^P(\omega)} / Z^P}{\sum_{l_s} e^{-\mathcal{E}^P(\omega)} / Z^P} = \frac{e^{-\mathcal{E}(\omega)} / Z}{\sum_{l_s} e^{-\mathcal{E}(\omega)} / Z} \end{aligned}$$

The sum extends over all possible values of  $L_s$  Hence we can say,  $\mathcal{G}_s^P = \mathcal{G}_s$ .

Thus, the posterior energy becomes,

$$\mathcal{E}^P(f, l) = \mathcal{E}(f, l) + \frac{1}{2\sigma^2} \|\mu - \Phi(g, \mathcal{D}_\psi(H(F)))\|^2 \quad (26)$$

**Corollary:** It can be observed that the second term is strictly positive. To generalize this further, we note that this term can be interpreted as a discrepancy measure between the likelihood and the prior. While the KL divergence is a common choice—being strictly positive—other discrepancy measures may also be employed. To demonstrate the similarity between the second term and the KL divergence, we proceed as follows:

$$\begin{aligned} \mathbb{P}(G = g \mid X = \omega) &= \frac{1}{(2\pi\sigma^2)^{M/2}} \exp\left\{-\frac{1}{2\sigma^2} \|\mu - \Phi(g, \mathcal{D}_\psi(H(F)))\|^2\right\} \\ \implies \log \mathbb{P}(G = g \mid X = \omega) &= -\frac{1}{2\sigma^2} \|\mu - \Phi(g, \mathcal{D}_\psi(H(F)))\|^2 + C \end{aligned}$$

Datasets	Methods	Evaluation Metrics								
		PSNR $\uparrow$	LPIPS $\downarrow$	MUSIQ $\uparrow$	CLIPQA $\uparrow$	SSIM $\uparrow$	DISTS $\downarrow$	FID $\downarrow$	NIQE $\downarrow$	MANIQA $\uparrow$
DIV2K-Val	S3Diff	23.40	<b>0.2571</b>	68.21	0.7007	0.5953	<b>0.1730</b>	<b>19.35</b>	4.7391	0.4538
	TSD-SR	23.02	0.2673	<b>71.69</b>	<b>0.7416</b>	0.5808	0.1821	29.16	<b>4.3244</b>	0.6192
	Add-SR	23.26	0.3623	63.39	0.5734	0.5902	0.2123	29.68	4.7610	0.5637
	OSDiff	23.72	0.2941	67.97	0.6683	0.6108	0.1976	26.32	4.7097	0.6148
	SinSR	24.41	0.3240	62.82	0.6471	0.6018	0.2066	35.57	6.0159	0.5386
	PassionSR	24.34	0.3440	51.19	0.4802	0.7097	0.2075	28.45	7.039	0.2267
	DMAPSR	<b>24.58</b>	0.2938	68.52	0.6842	<b>0.6112</b>	0.1962	27.19	4.6721	<b>0.6416</b>
RealSR	S3Diff	25.03	<b>0.2699</b>	67.89	0.6722	0.7321	<b>0.1996</b>	<b>108.88</b>	5.3311	0.4563
	TSD-SR	24.81	0.2743	<b>71.19</b>	<b>0.7160</b>	0.7172	0.2104	114.45	<b>5.1298</b>	0.6347
	Add-SR	24.79	0.3091	66.18	0.5722	0.7077	0.2191	132.05	5.5440	0.6098
	PassionSR	22.52	0.4913	43.21	0.3089	0.6255	0.3185	129.54	5.706	0.2396
	OSDiff	25.15	0.2921	69.09	0.6693	0.7341	0.2128	123.49	5.6476	0.6326
	SinSR	26.28	0.3188	60.80	0.6122	0.7347	0.2353	135.93	6.2872	0.5385
	DMAPSR	<b>26.29</b>	0.2918	69.81	0.6651	<b>0.7426</b>	0.2178	127.92	5.4104	<b>0.6492</b>
DRealSR	S3Diff	26.89	0.3122	64.19	0.7122	0.7469	0.2120	<b>119.86</b>	6.1647	0.4508
	TSD-SR	27.77	0.2967	<b>66.62</b>	<b>0.7344</b>	0.7559	0.2136	134.98	<b>5.9131</b>	0.5874
	Add-SR	27.77	0.3196	60.85	0.6188	0.7722	0.2242	150.18	6.9321	0.5490
	SinSR	28.36	0.3665	55.33	0.6383	0.7515	0.2485	170.57	6.9907	0.4884
	OSDiff	27.92	0.2968	64.65	0.6963	0.7835	0.2165	135.30	6.4902	0.5899
	DMAPSR	<b>28.32</b>	<b>0.2957</b>	64.97	0.6975	<b>0.7842</b>	<b>0.2096</b>	139.75	6.3245	<b>0.6172</b>

Table 5: We conduct a quantitative comparison of DMAPSR with state-of-the-art Real-ISR models based on one-step diffusion frameworks across various datasets. The best-performing method is highlighted in bold, while the second-best result is indicated with an underline.

Where  $C = -\frac{M}{2} \log(2\pi\sigma^2)$  as  $X$  is independent of  $\mathcal{N}$ . Now, taking  $\langle h(X) \rangle = E_X[h(X)]$  we can write the above as,

$$\begin{aligned}
\text{KL}[\mathbb{P}(X = \omega) || \mathbb{P}(G = g | X = \omega)] &= \langle \log \mathbb{P}(X = \omega) \rangle - \langle \log \mathbb{P}(G = g | X = \omega) \rangle \\
&= \frac{1}{2\sigma^2} \langle ||\mu - \Phi(g, \mathcal{D}_\psi(H(F)))||^2 \rangle + C - \langle -\frac{U(\omega)}{Z} \rangle \\
&= \frac{1}{2\sigma^2} \langle ||\mu - \Phi(g, \mathcal{D}_\psi(H(F)))||^2 \rangle + C
\end{aligned}$$

Hence, effectively we can write the posterior energy as,

$$\mathcal{E}^P(f, l) = \mathcal{E}(f, l) + \text{KL}[\mathbb{P}_{\mathbf{Y}|\mathbf{X}}(g|f, l) || \mathbb{P}_{\mathbf{X}}(f, l)] \quad (27)$$

## ADDITIONAL RESULTS:

We present additional comparative results with existing diffusion model-based methods in Fig. 4. Our method demonstrates superior performance, particularly in recovering fine structures such as artificial flower petals, leaf textures, and cloth patterns, under both ground truth and non-ground truth scenarios. In addition, we provide further quantitative comparisons with state-of-the-art one-step diffusion-based image super-resolution methods, as reported in Table 5.

## VISUALIZATION OF LINE FIELDS:

We present the horizontal and vertical line fields in forward and backward directions generated during inference in Fig. 5.

## USAGE OF LARGE LANGUAGE MODEL:

We have utilized a large language model (LLM) solely for grammatical correction, word choice refinement, and improving sentence phrasing.

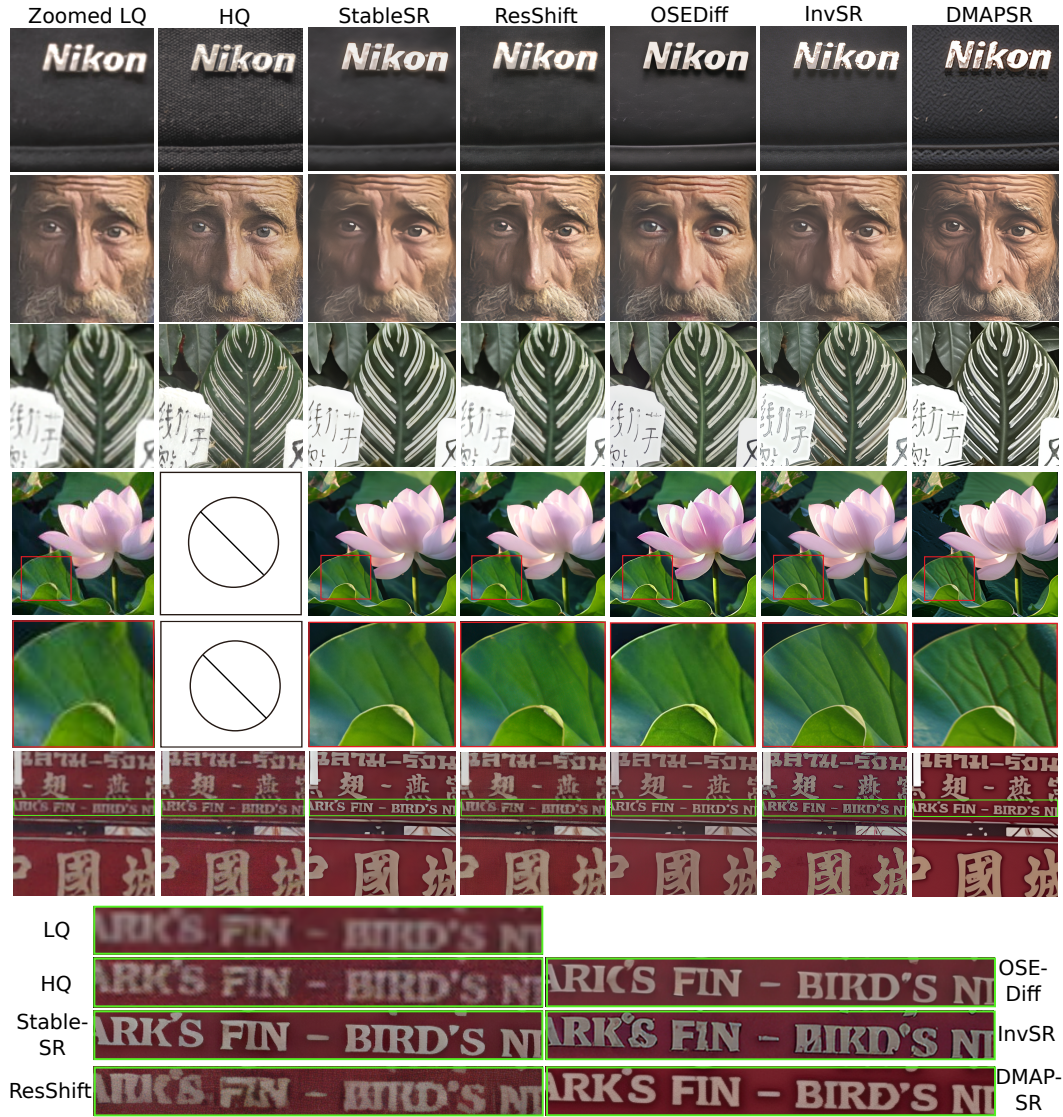


Figure 4: Qualitative visual comparisons of Real-ISR methods are presented. Note that the third example lacks a corresponding high-quality ground truth image. Please zoom in for a clearer view.



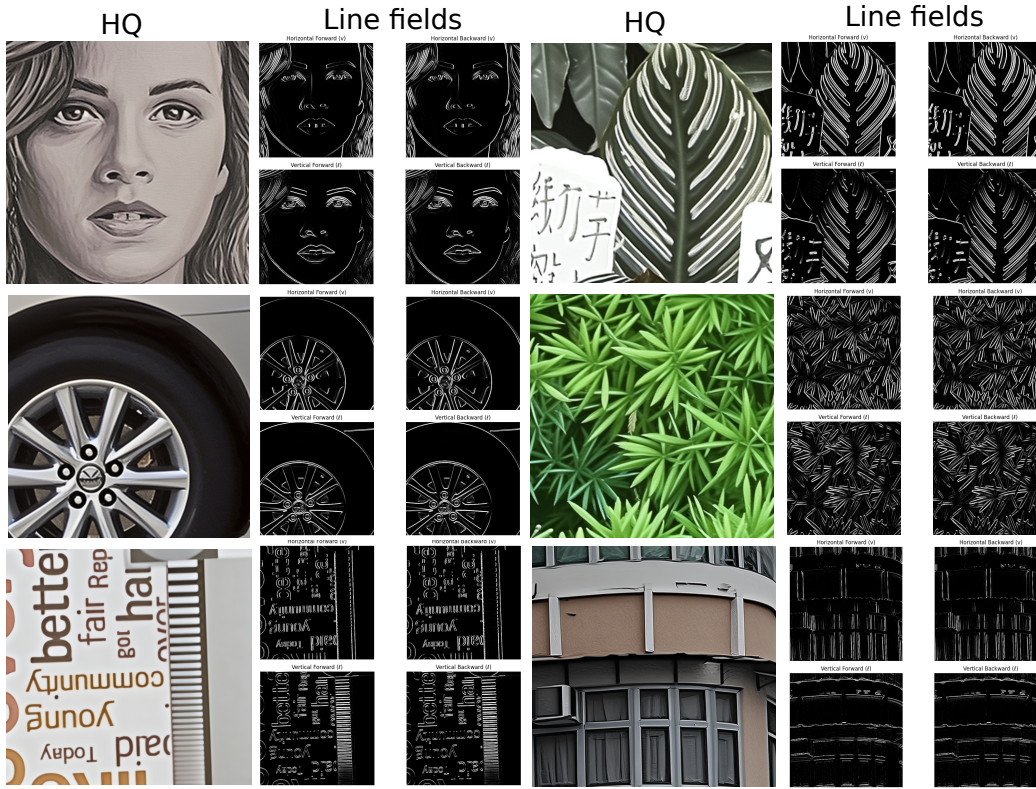


Figure 5: Horizontal and vertical line fields in both forward and backward directions are shown alongside the generated HQ image. Please zoom in for a clearer view.